Electronic Supplementary Material (ESI) for Physical Chemistry Chemical Physics

Supplementary Information

Distance measurements in Au nanoparticles functionalized with nitroxide radicals and Gd^{3+}-DTPA chelate complexes

Maxim Yulikov,[*a] Petra Lueders,[a] Muhammad Farooq Warsi,[b,c] Victor Chechik[*b] and Gunnar Jeschke[a]

[a] *Laboratory of Physical Chemistry, ETH Zurich, Wolfgang Pauli Str.10, 8093, Zurich, Switzerland;*
[b] *Department of Chemistry, University of York, Heslington, York YO10 5DD, UK.*
[c] *Present address: Chemistry Department, Baghdad-ul-Jaded Campus, The Islamia University of Bahawalpur, Bahawalpur-63100, Pakistan*
E-mail: (a) maxim.yulikov@phys.chem.ethz.ch; (b) victor.chechik@york.ac.uk

Contents:

1. Characterization of Au-nanoparticles

Determination of Nitroxide Radical Concentration

The number of active nitroxides per particle was estimated by continuous-wave (CW) EPR measurements and the synthesis (nitroxide labelling step) was adjusted to obtain a modulation depth in nitroxide-nitroxide DEER in the order of 0.15-0.2, which corresponded to an average of 0.3-0.4 active nitroxides per particle, assuming a uniform distribution of active nitroxides over all nanoparticles.

The concentration of the active nitroxides at the gold nanoparticle surface was estimated by double integration of CW EPR spectra. In the first instance, a calibration curve was set up by plotting known concentrations of nitroxide radicals (TEMPO) *versus* the double integrals of their CW EPR spectra (Fig. S1). This calibration curve was used for estimating active nitroxide radical at the nanoparticle surface before and after the deprotection step. The deprotection of t-butyl ester groups of DTPA ligand at the nanoparticle surface led to ~70-80% loss of nitroxides from AuNPs surface. After the deprotection step the 0.2 nitroxides per particle concentration was estimated by double integration of CW EPR spectra.

In Table 1 the modulation depths obtained from DEER measurements of the four studied samples are listed. The modulation depth for different samples ranges from 0.12 to 0.23, which implies an average of 0.25-0.45 active nitroxides per AuNP, assuming a completely random distribution of paramagnetic species over all AuNPs. The agreement between CW and DEER determination of the number of active nitroxides per particle is reasonably good, taking into account polydispersity of the samples. An additional effect that could have contributed to the discrepancy between the two methods is the strong enhancement of the relaxation of nitroxide radicals induced by Gd^{3+} ions at RT. This could have broadened the EPR signals for the pairs with Gd^{3+}-

nitroxide distances below ~2 nm and thus reduced apparent number of spins per AuNP obtained from double integration.

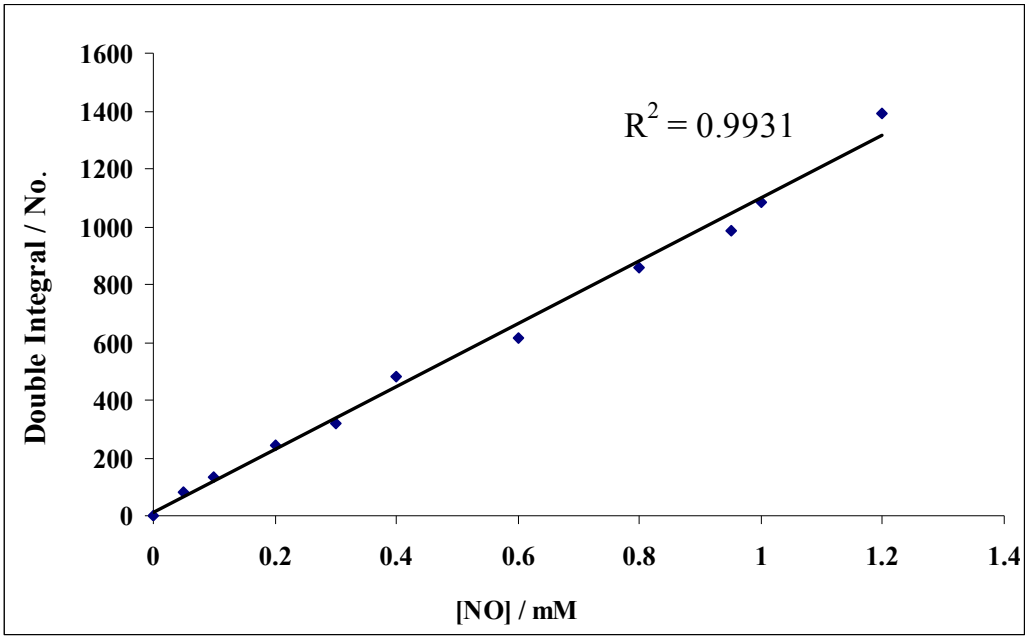

Figure S1: Calibration curve for determination of the nitroxide concentration. The experimental reference data were best fitted with the linear function f([NO]) = 1086·[NO] + 10.15.

Table 1. X-band DEER modulation depths for samples studied.

Sample	NO-NO DEER Mod. depth	Gd-NO DEER Mod. depth
32% La	0.23	-
0% Gd	0.12	-
2% Gd	0.23	0.18
4% Gd	0.15	0.15

Determination of DTPA-based Ligand Concentration

After spin-labeling and deprotection, the numer of DTPA ligands at the nanoparticle surface could be estimated by Gd-loading with xylenol orange using UV/Vis spectroscopy. Before spin labeling, the composition of nanoparticles was $\mathbf{Au_{439}L_{88}}$, after spin labeling the estimated composition was $\mathbf{Au_{439}L_{80}NO_{0.2\text{-}0.4}}$. This composition is estimated from xylenol orange titration (concentration of DTPA-based chelators after spin labeling & deprotection), TEM (average size of AuNPs) and TGA data (weight fraction of organic material).

TEM of AuNPs protected by DTPA ligand 5

TEM image (Figure S2) of AuNPs showed well dispersed nanoparticles with average diameter 2.42 ± 0.34 nm.

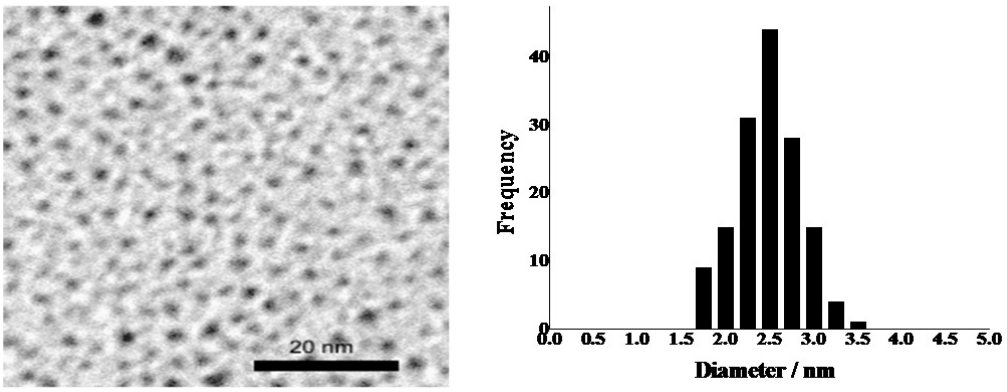

Figure S2: TEM image (left) and size distribution histogram (right) of AuNPs protected by DTPA ligand.

2. Fitting of the ZFS parameter *D* from Gd^{3+} Echo Detected (ED) EPR spectra

In order to obtain the characteristic value of the ZFS-parameter D for the studied Gd^{3+} complexes we performed a series of model calculations of EPR spectra for Gaussian distributions of D with different mean values (300, 600, 1100, 1500 and 2000 MHz) and different widths ($\sigma=D/100$, $D/10$, $D/5$ and $D/3$) and compared them to the experimental Gd^{3+} ED EPR spectra. The ratio E/D was distributed in all cases according to the same probability function $P(E/D)=(E/D)-2\cdot(E/D)^2$ (see main text for more details). The two upper plots in Figure S3 show X- and Q-band EPR spectra simulated for different $\langle D\rangle$ = 300, 600, 1100, 1500 and 2000 MHz, with $\sigma=D/10$ in all cases. One can see that the spectra computed for $\langle D\rangle$ =1500 MHz fit rather well to the experimental data. The lower two plots show how the Gd^{3+} EPR spectrum changes upon the increase of the width of Gaussian distribution for D-values. The best agreement with the experimental spectra is obtained for simulations with the value of $\sigma=D/5$ and $\sigma=D/10$. Experimental ED EPR spectra of Gd^{3+} complexes were measured at 10 K.

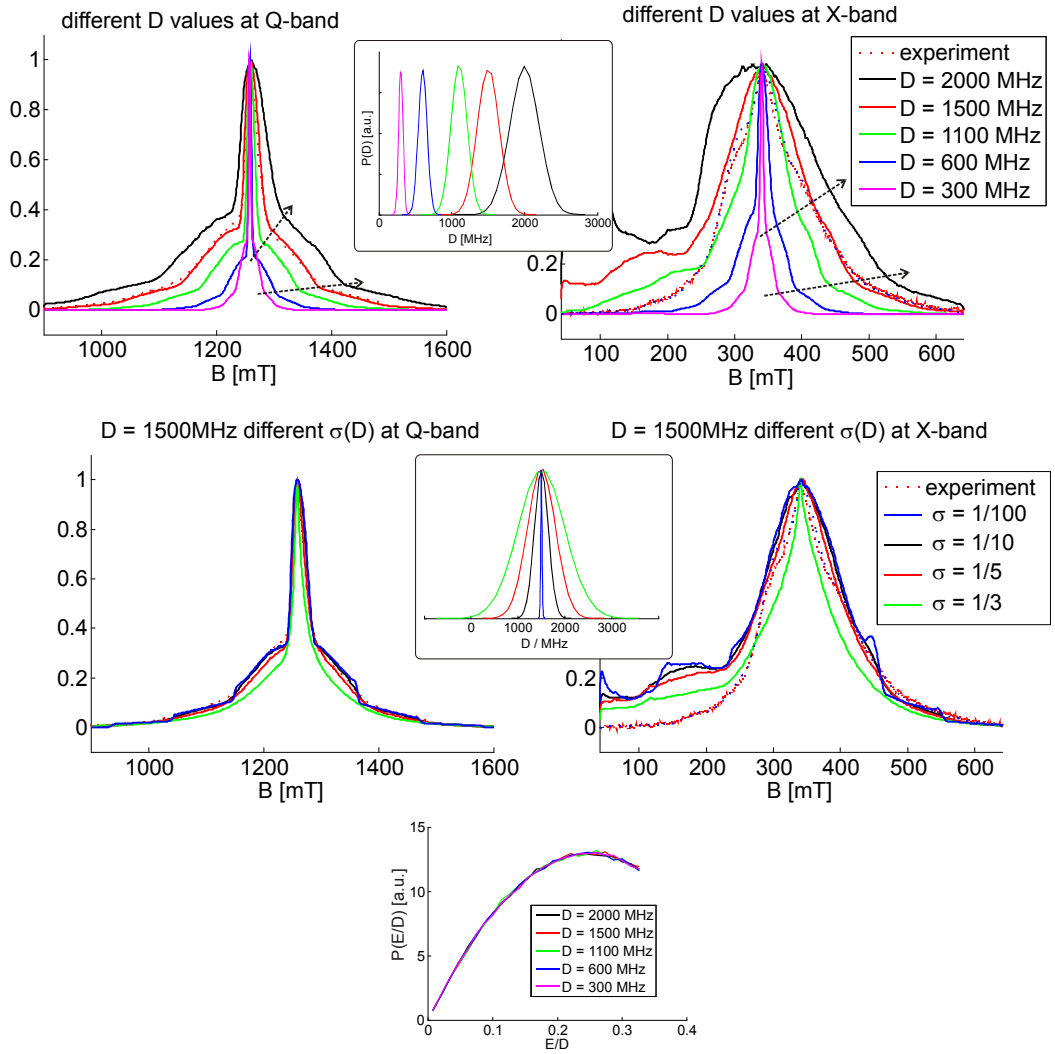

Figure S3. Simulations of EPR spectra of Gd^{3+} centers and their comparison to the experimentally detected ED EPR spectra of Gd^{3+} complexes with DTPA-based linker molecules: left: Q-band spectra, right: X-band spectra. Spectra were simulated with second rank ZFS terms included, the corresponding distributions of D and E parameters of ZFS term are shown in the insets. For the discussion of the distribution of E/D, see the main text of the article.

3. Numeric calculations of dipolar frequencies for different ZFS parameters

Figures S4-S14 illustrate further details of the performed analysis of dipolar frequency distortions. In particular Figures S10, S12-S14 allow to correlate qualitatively the shape of Gd^{3+} EPR spectrum with the distortions for $\Delta m_{\parallel}$ and $\Delta m_{\perp}$, with characteristic shapes of dipolar frequency patterns (distorted Pake patterns), with refocusing of dipolar oscillations in DEER traces and with distortions of obtained distances.

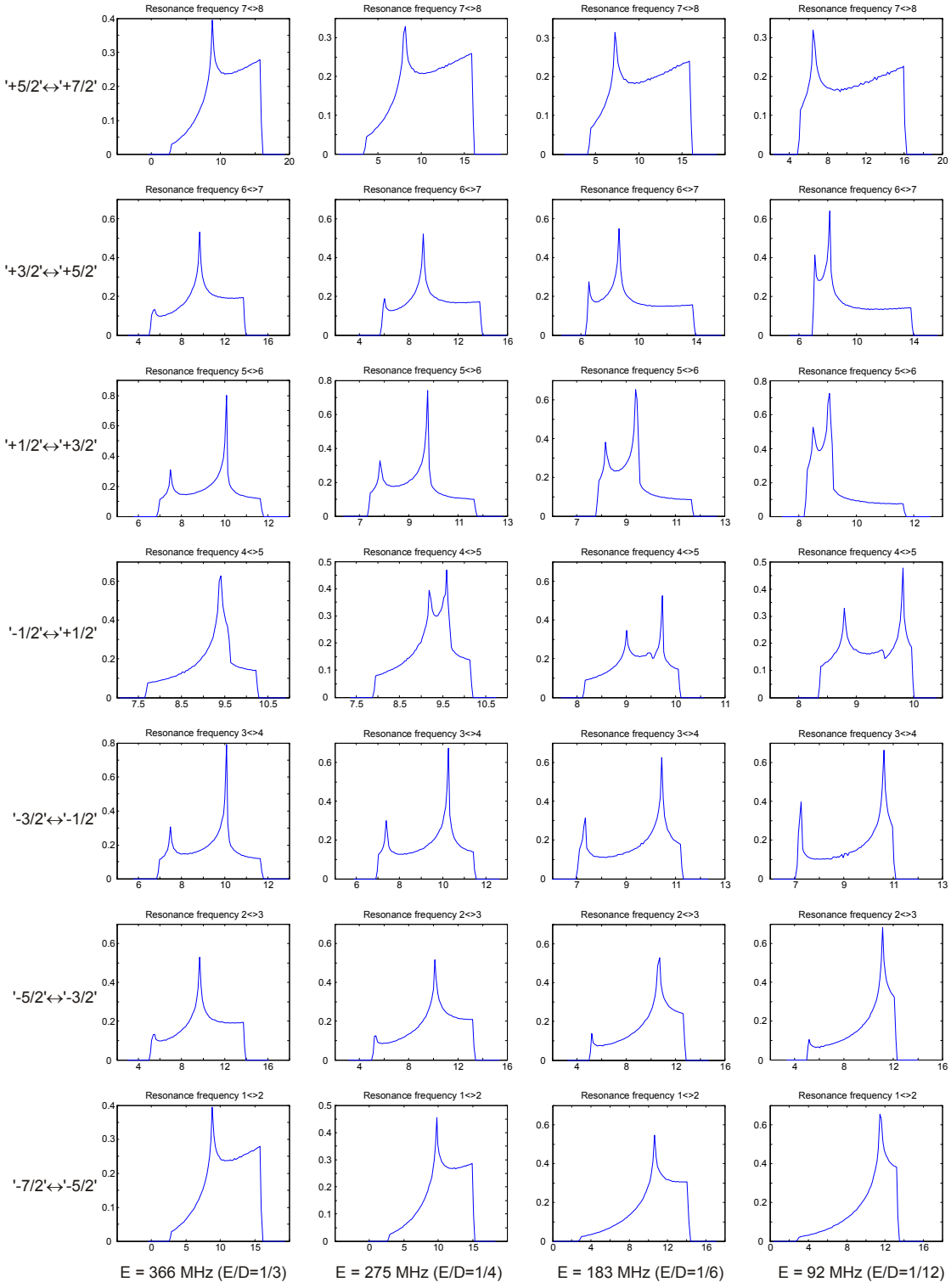

Figure S4. Transition-separated distributions of resonance frequencies for D=1100 MHz with E=D/3, D/4, D/6 and D/12. A regular triangular grid of 80200 points was used in this calculation. Level sorting: 1 = |-7/2>; 8 = |+7/2>. On the x-axis of each graph the resonance frequency is given in GHz. The y-axis of each graph is the probability density in arbitrary units.

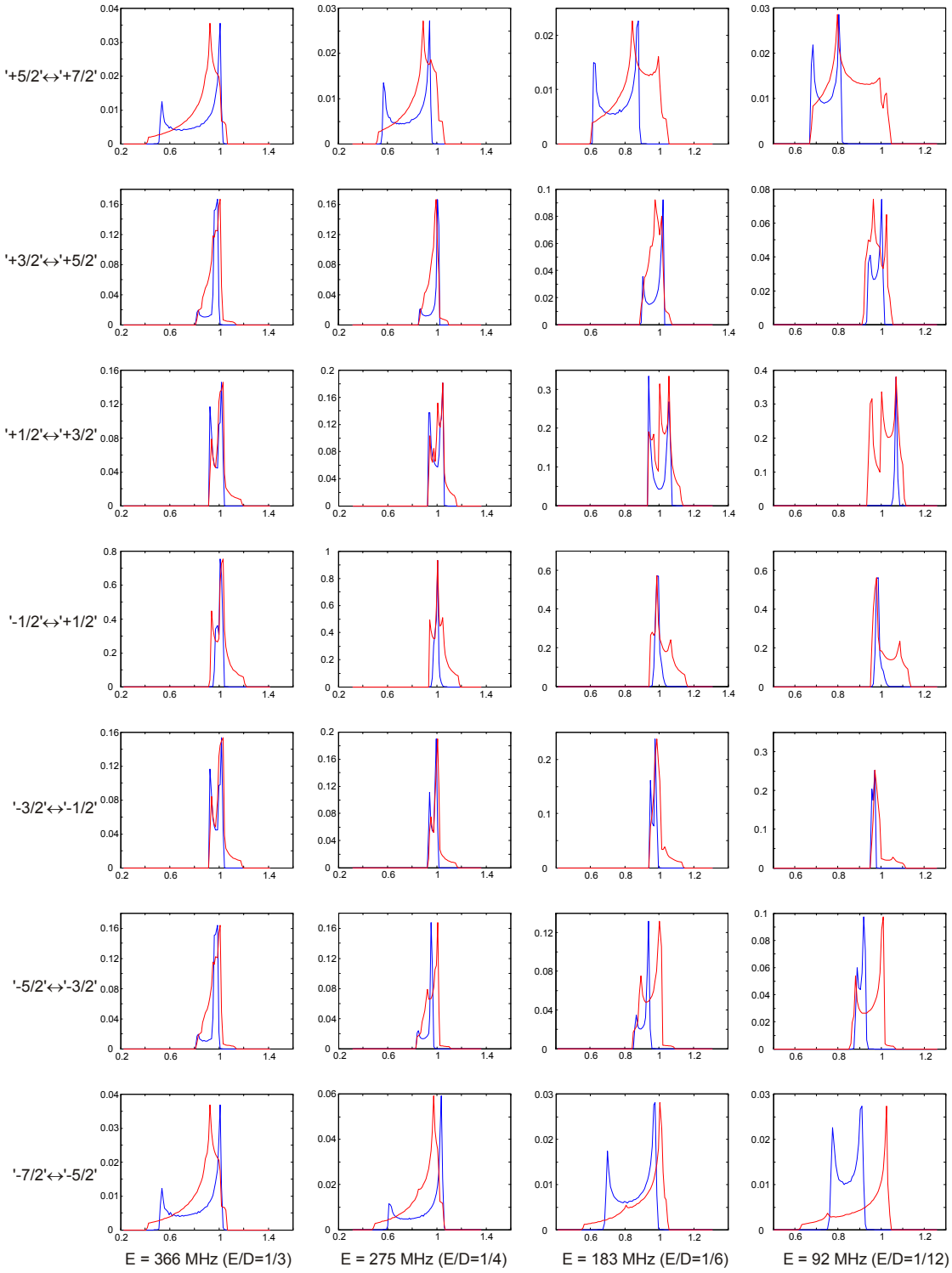

Figure S5. Transition-separated distributions of $\Delta m_{\|}$ for D=1100 MHz with E=D/3, D/4, D/6 and D/12. A regular triangular grid of 80200 points was used in this calculation. On the x-axis of each graph the dimensionless value of $\Delta m_{\|}$ is given. The y-axis of each graph is the probability density in arbitrary units, identical for red curves in all graphs in the same column. In each graph the blue curve is vertically stretched for the same maximum value as the red curve. Excitation was set to be at 9.474 GHz with 100 MHz width of Gaussian excitation profile. Red: full distributions, blue: distributions corrected for the given excitation profile.

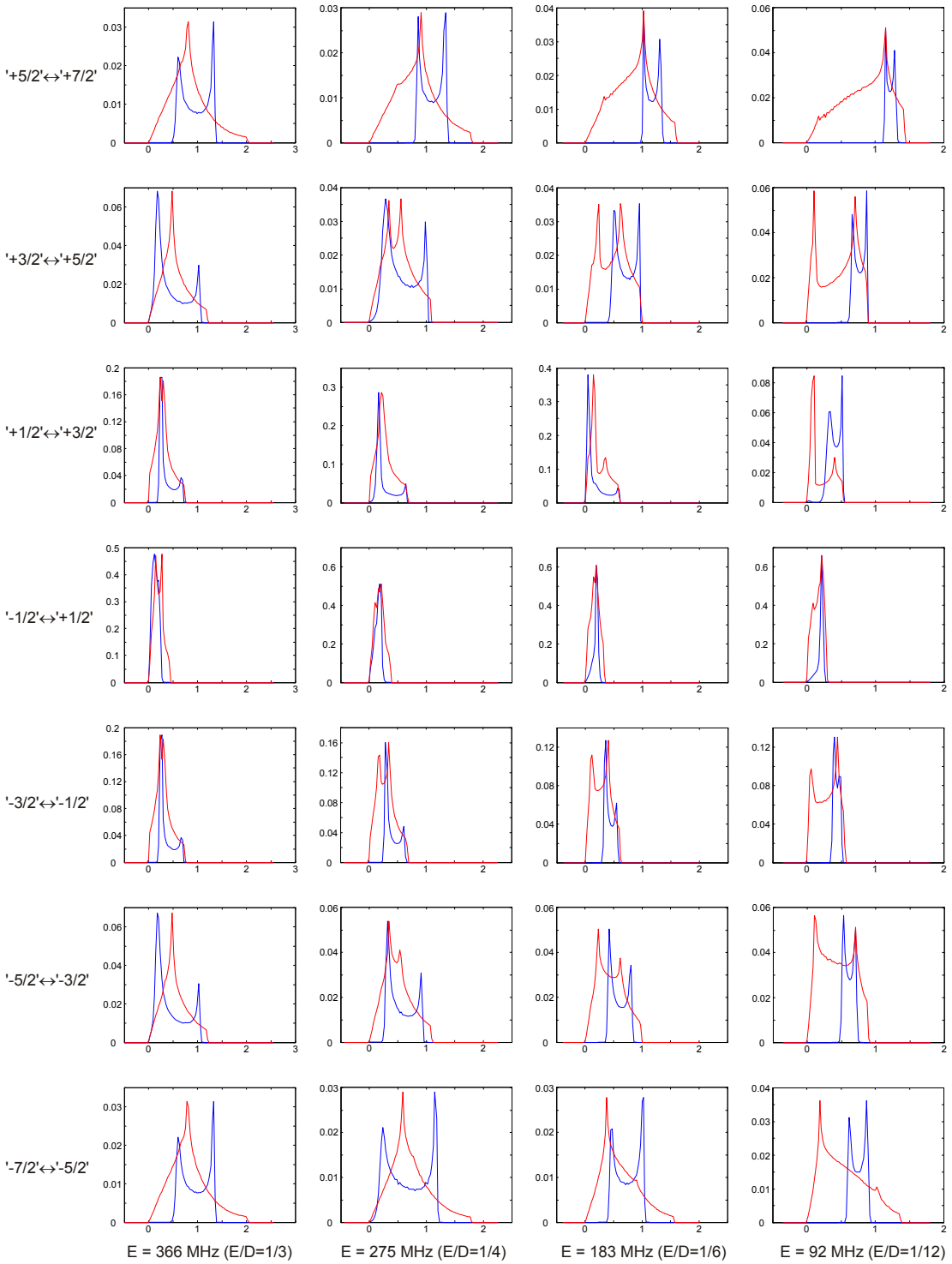

Figure S6. Transition-separated distributions of $\Delta m_{\perp}$ for D=1100 MHz with E=D/3, D/4, D/6 and D/12. A regular triangular grid of 80200 points was used in this calculation. On the x-axis of each graph the dimensionless value of $\Delta m_{\perp}$ is given. The y-axis of each graph is the probability density in arbitrary units, identical for red curves in all graphs in the same column. In each graph the blue curve is vertically stretched for the same maximum value as the red curve. Excitation was set to be at 9.474 GHz with 100 MHz width of Gaussian excitation profile. Red: full distributions, blue: distributions corrected for the given excitation profile.

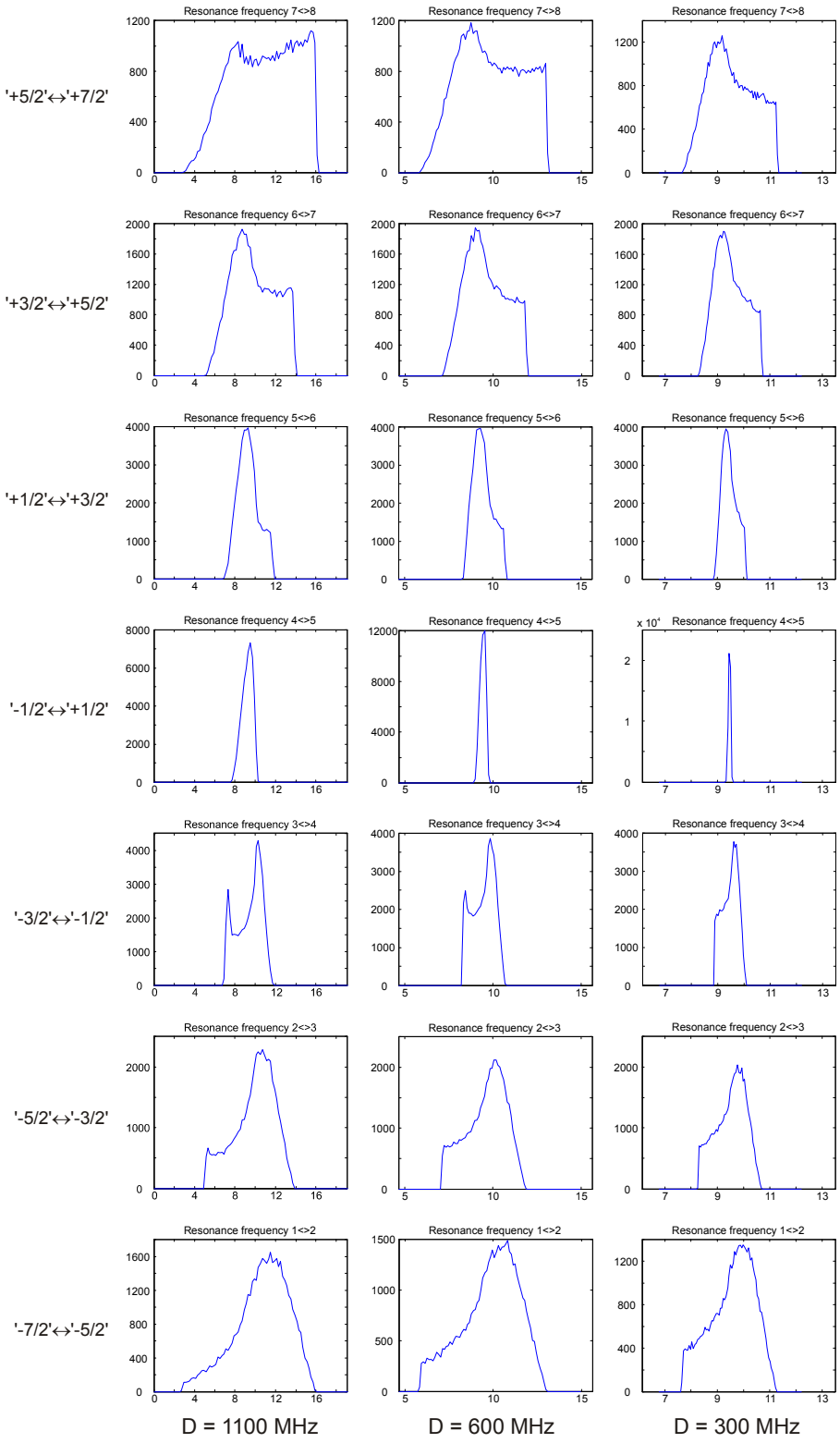

Figure S7. Transition-separated distributions of resonance frequencies for D=1100, 600 and 300 MHz. The values of E/D are distributed as described in the main text of the article. Summation over an ensemble of random values of two polar angles and E/D with 50000 points was used in each calculation. Level sorting: 1 = |-7/2>; 8 = |+7/2>. On the x-axis of each graph the resonance frequency is given in GHz. The y-axis of each graph is the probability density in arbitrary units.

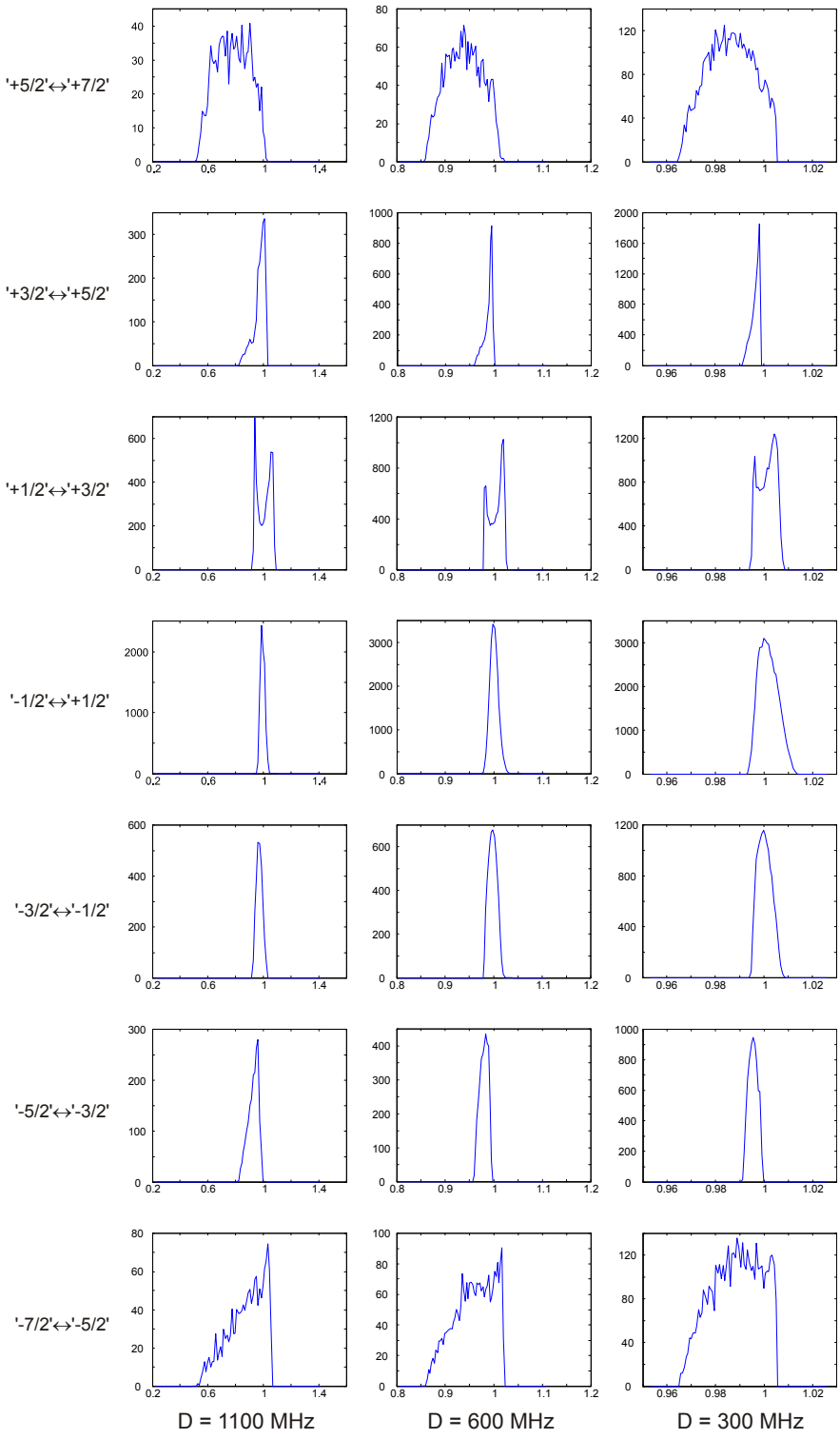

Figure S8. Transition-separated distributions of $\Delta m_{||}$ for D=1100, 600 and 300 MHz. The values of E/D are distributed as described in the main text of the article. Summation over an ensemble of random values of two polar angles and E/D with 50000 points was used in each calculation. On the x-axis of each graph the dimensionless value of $\Delta m_{||}$ is given. The y-axis of each graph is the probability density in arbitrary units, identical for all graphs in the same column. Excitation was set to be at 9.474 GHz with 100 MHz width of Gaussian excitation profile. Distributions corrected for this excitation profile are shown.

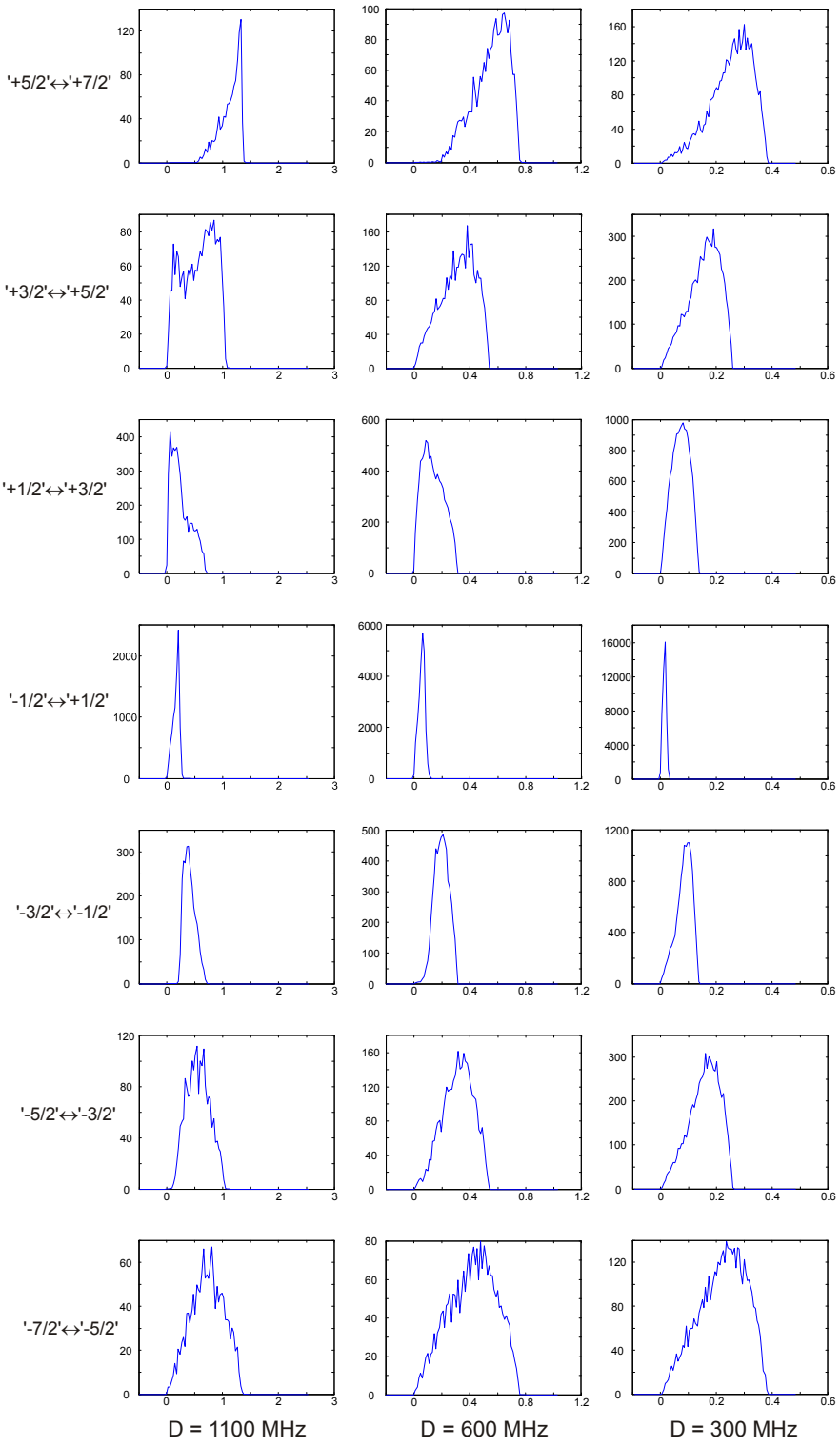

Figure S9. Transition-separated distributions of $\Delta m_{\perp}$ for D=1100, 600 and 300 MHz. The values of E/D are distributed as described in the main text of the article. Summation over an ensemble of random values of two polar angles and E/D with 50000 points was used in each calculation. On the x-axis of each graph the dimensionless value of $\Delta m_{\perp}$ is given. The y-axis of each graph is the probability density in arbitrary units, identical for all graphs in the same column. Excitation was set to be at 9.474 GHz with 100 MHz width of Gaussian excitation profile. Distributions corrected for this excitation profile are shown.

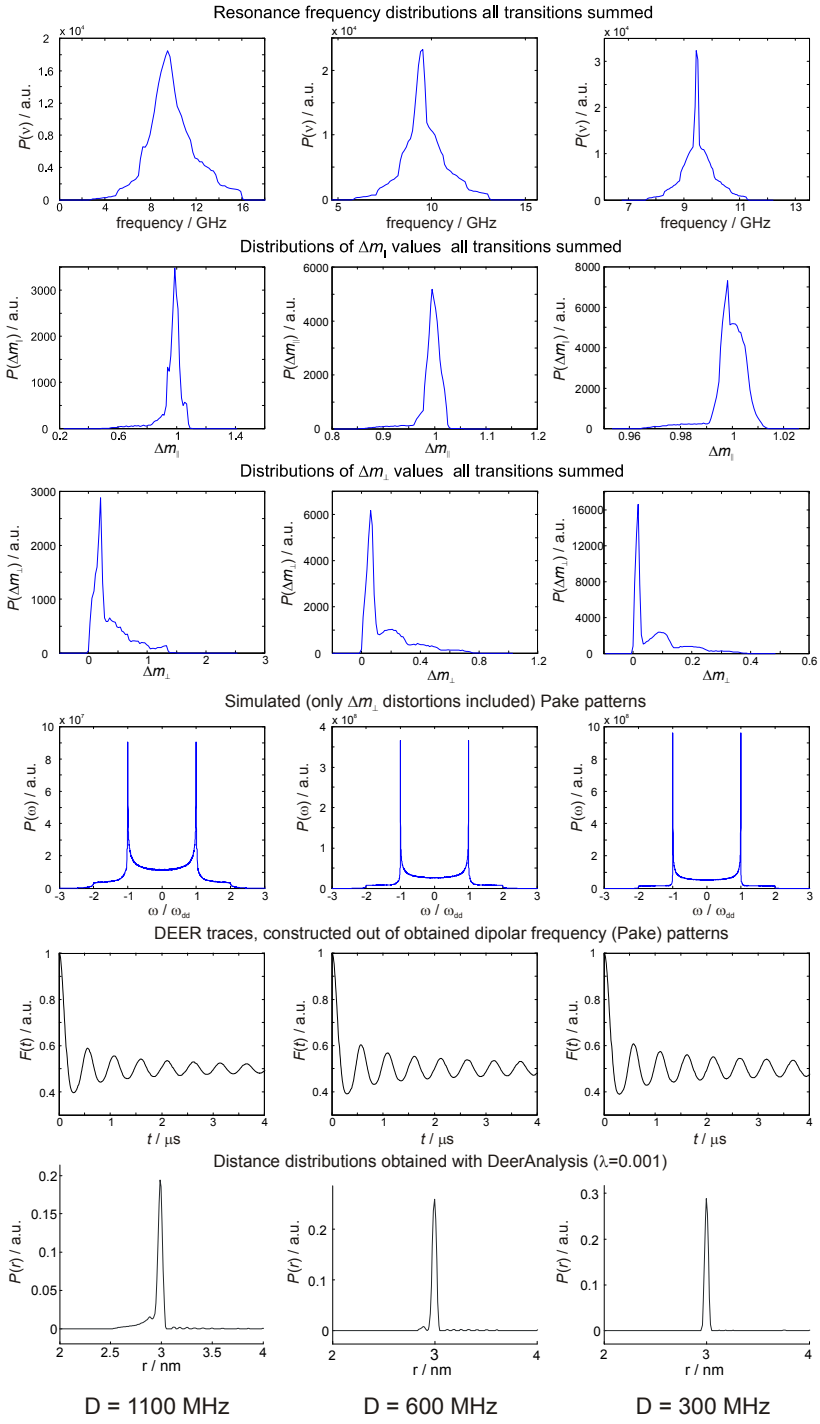

Figure S10. Analysis of $\Delta m_{\perp}$-induced distortions in DEER based distance measurements for D=1100, 600 and 300 MHz. The values of E/D are distributed as described in the main text of the article. Summation over an ensemble of random values of two polar angles and E/D with 50000 points was used in each calculation. DEER traces were generated by setting the dipolar frequency for the case $\Delta m_{\perp}$=0 and $\Delta m_{||}$=1.0 to correspond to the distance of 3.0 nm. The shapes of obtained distance distributions illustrate the distortions of the distance measurement due to ZFS interaction. In the limit of vanishing ZFS a delta-function type distribution at 3.0 nm is expected. Distance distributions were obtained by fitting the DEER traces with DeerAnalysis 2009 software with the model free fit routine. The distributions, corresponding to a Tikhonov regularization parameter λ=0.001 are shown.

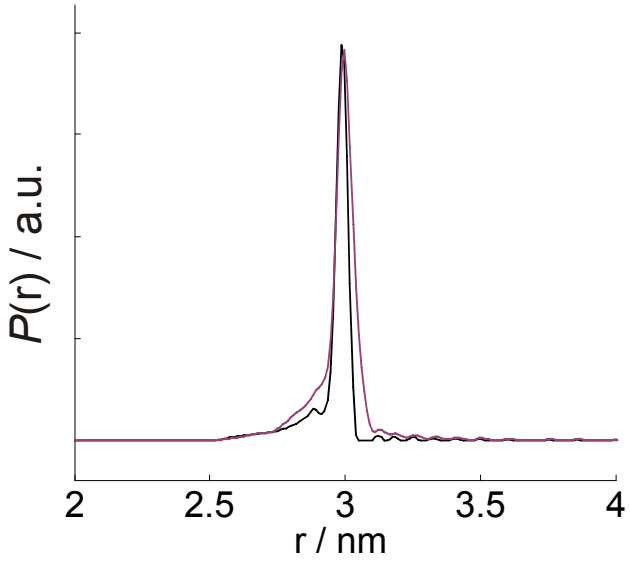

Figure S11. Analysis of distortions in DEER based distance measurements for D=1100 MHz. The values of E/D are distributed as described in the main text of the article. Black: the distance pattern obtained if only the distortions of $\Delta m_{\perp}$ are taken into account. Purple: the distance pattern obtained if distortions of both $\Delta m_{\perp}$ and $\Delta m_{\parallel}$ are taken into account.

Figure S12. Analysis of full, $\Delta m_{\|}$- and $\Delta m_{\perp}$-induced distortions in DEER based distance measurements for fixed D = 1100, 1500 and 2000 MHz.

Figure S13. Analysis of full, $\Delta m_{\|}$- and $\Delta m_{\perp}$-induced distortions in DEER based distance measurements for Gaussian distributions of ZFS parameter D with $\langle D \rangle$ = 1100, 1500 and 2000 MHz and with $\sigma(D) = D/10$.

Figure S14. Analysis of full, $\Delta m_{\|}$- and $\Delta m_{\perp}$-induced distortions in DEER based distance measurements for Gaussian distributions of ZFS parameter D with $\langle D \rangle$ = 1100, 1500 and 2000 MHz and with $\sigma(D) = D/4$.

Comments on all three figures: The values of E/D are distributed as described in the main text of the article. Summation over an ensemble of random values of two polar angles and E/D with 50000 points was used in each calculation. DEER traces were generated by setting dipolar frequency for $\Delta m_{\perp}$=0 and $\Delta m_{\|}$=1.0 to correspond to the distance of 3.0 nm. The shapes of obtained distance distributions illustrate the distortions of the distance measurement due to ZFS interaction. In the limit of vanishing ZFS a delta-function type distribution at 3.0 nm is expected. Distance distributions were obtained by fitting the DEER traces with DeerAnalysis 2009 software with the model free fit routine. The distance distributions, corresponding to a Tikhonov regularization parameter λ=0.001 are shown. Excitation was set to be at 9.474 GHz (X-band) with 100 MHz width of Gaussian excitation profile. Distributions of $\Delta m_{\perp}$ and $\Delta m_{\|}$ corrected for this excitation profile are shown.

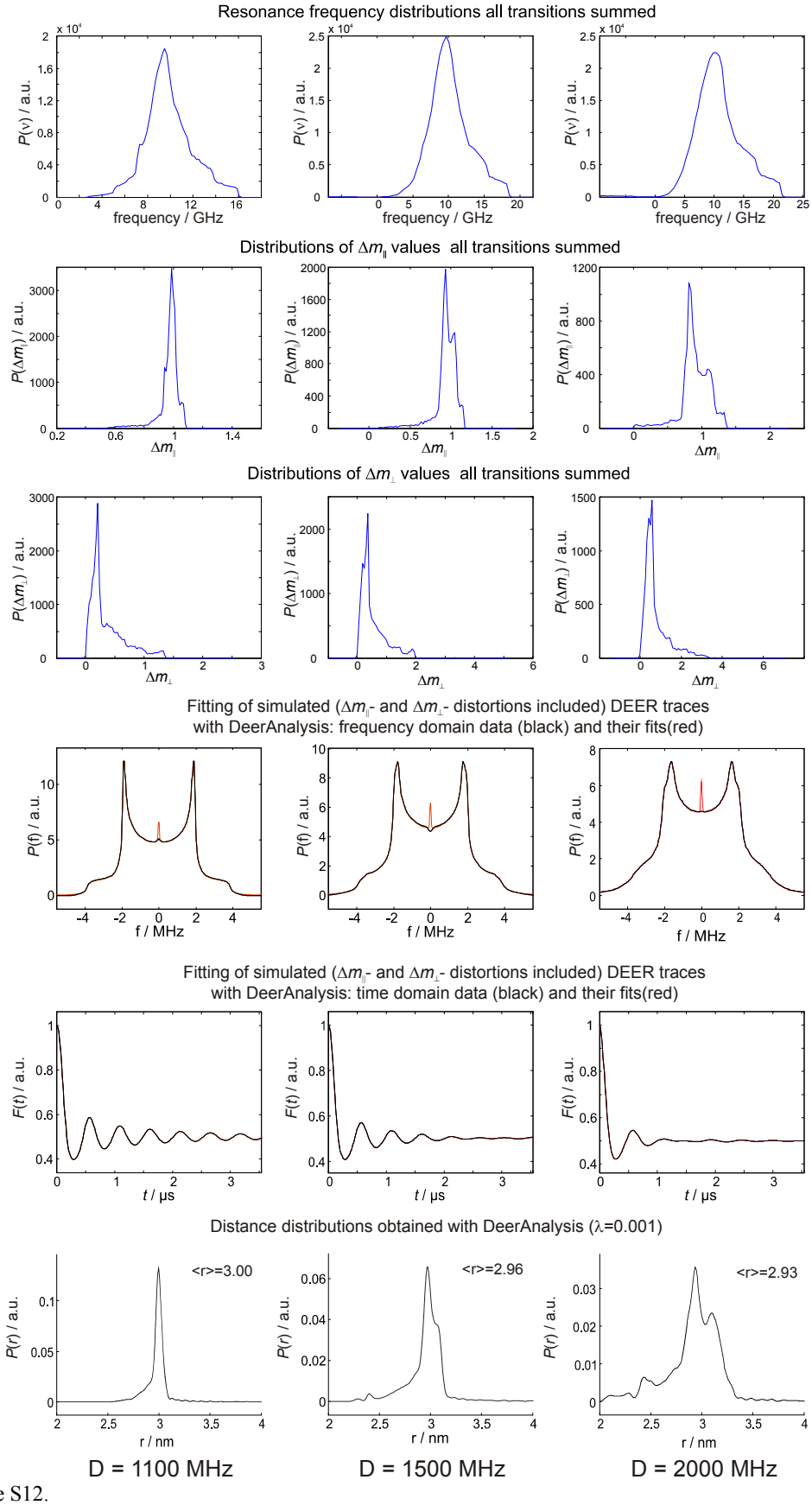
Resonance frequency distributions all transitions summed
P(ν) / a.u.
frequency / GHz
Distributions of Δm‖ values all transitions summed
P(Δm‖) / a.u.
Δm‖
Distributions of Δm⊥ values all transitions summed
P(Δm⊥) / a.u.
Δm⊥
Fitting of simulated (Δm‖- and Δm⊥- distortions included) DEER traces
with DeerAnalysis: frequency domain data (black) and their fits(red)
P(f) / a.u.
f / MHz
Fitting of simulated (Δm‖- and Δm⊥- distortions included) DEER traces
with DeerAnalysis: time domain data (black) and their fits(red)
F(t) / a.u.
t / µs
Distance distributions obtained with DeerAnalysis (λ=0.001)
P(r) / a.u.
r / nm
<r>=3.00
<r>=2.96
<r>=2.93
D = 1100 MHz
D = 1500 MHz
D = 2000 MHz

Figure S12.

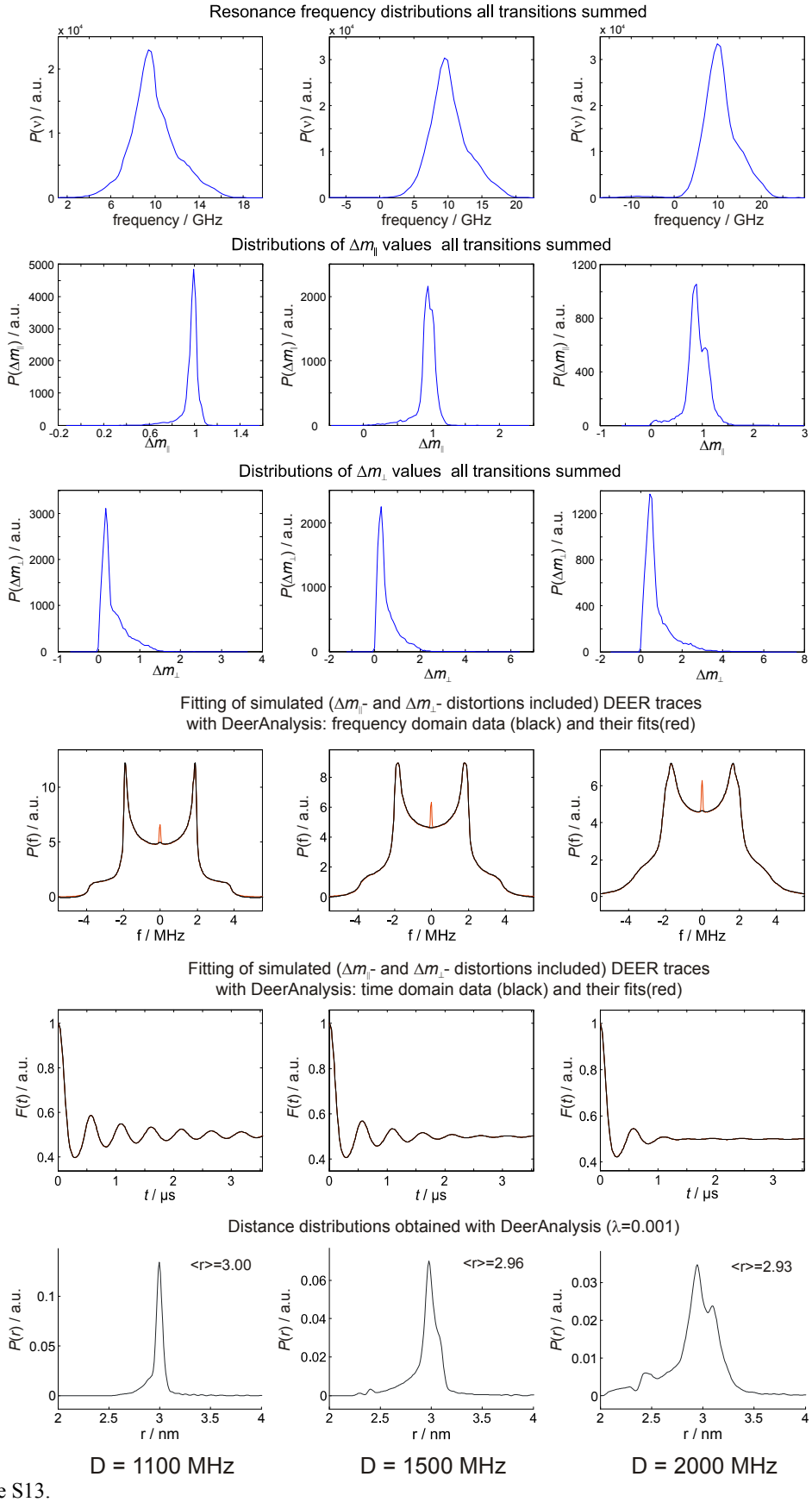
Resonance frequency distributions all transitions summed
P(ν) / a.u.
frequency / GHz
Distributions of Δm‖ values all transitions summed
P(Δm‖) / a.u.
Δm‖
Distributions of Δm⊥ values all transitions summed
P(Δm⊥) / a.u.
Δm⊥
Fitting of simulated (Δm‖- and Δm⊥- distortions included) DEER traces
with DeerAnalysis: frequency domain data (black) and their fits(red)
P(f) / a.u.
f / MHz
Fitting of simulated (Δm‖- and Δm⊥- distortions included) DEER traces
with DeerAnalysis: time domain data (black) and their fits(red)
F(t) / a.u.
t / µs
Distance distributions obtained with DeerAnalysis (λ=0.001)
P(r) / a.u.
r / nm
<r>=3.00
<r>=2.96
<r>=2.93
D = 1100 MHz
D = 1500 MHz
D = 2000 MHz

Figure S13.

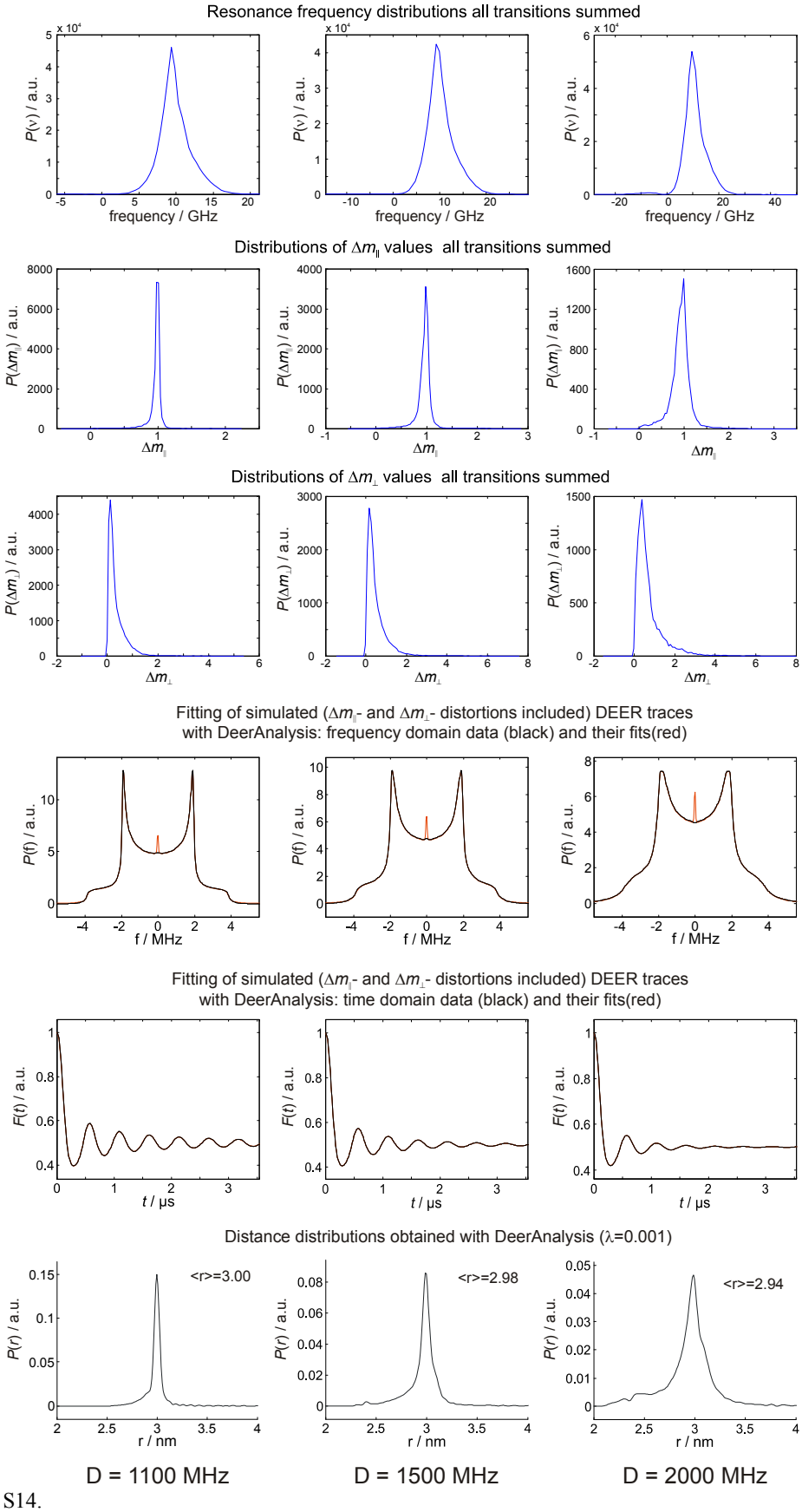
Resonance frequency distributions all transitions summed
P(ν) / a.u.
frequency / GHz
Distributions of Δm‖ values all transitions summed
P(Δm‖) / a.u.
Δm‖
Distributions of Δm⊥ values all transitions summed
P(Δm⊥) / a.u.
Δm⊥
Fitting of simulated (Δm‖- and Δm⊥- distortions included) DEER traces
with DeerAnalysis: frequency domain data (black) and their fits(red)
P(f) / a.u.
f / MHz
Fitting of simulated (Δm‖- and Δm⊥- distortions included) DEER traces
with DeerAnalysis: time domain data (black) and their fits(red)
F(t) / a.u.
t / µs
Distance distributions obtained with DeerAnalysis (λ=0.001)
P(r) / a.u.
r / nm
<r>=3.00
<r>=2.98
<r>=2.94
D = 1100 MHz
D = 1500 MHz
D = 2000 MHz

Figure S14.

4. Evaluation of the signal-to-noise ratios in nitroxide-nitroxide, Gd^{3+}-nitroxide and Gd^{3+}- Gd^{3+} DEER measurements.

The sensitivity of Gd^{3+}-nitroxide and nitroxide-nitroxide DEER experiments was compared on the 2% Gd^{3+} loaded sample. Four DEER traces of the same length of 2.8 μs were measured for this purpose. Both at X and at Q band all pulses in DEER sequence were set to 12 ns. Further details are listed in the Table 2.

The sensitivity of Gd^{3+}-nitroxide and Gd^{3+}- Gd^{3+} DEER experiments was compared on the 4% Gd^{3+} loaded sample. DEER traces of the same length of 3 μs were measured for this purpose (pulse settings as for Table 2). Further details are listed in the Table 3.

Table 2. Comparison of the sensitivity of Gd^{3+}-nitroxide and nitroxide-nitroxide DEER experiments. Abbreviations: srt – shot repetition time; rmsd – root mean square deviation; spp – shots per point; pcp – phase cycling protocol (this includes two step cycling of the first pulse phase and 8 step ESEEM averaging protocol); S/N – signal to noise ratio. Estimated number of paramagnetic centres per AuNP is 0.4 for nitroxide radicals and 1.6 for Gd^{3+} centres.

	NO-NO @ Xband	NO-NO @ Qband	Gd^{3+}-NO @ Xband	Gd^{3+}-NO @ Qband
Modulation depth	0.23	0.20	0.18	0.17
srt [μs]	1632.00 us	1632.00 us	1006.74 us	1020.00 us
point per trace	355	355	355	355
spp in single trace	100	100	200	200
length of pcp	16	16	16	16
scans	89	89	40	40
rmsd	2.6e-002	6.1e-003	7.2e-003	2.4e-003
S/N	8.7	32.7	24.4	70.2
S/N per shot	6.1e-005	2.3e-004	1.9e-004	5.5e-004

Table 3. Comparison of the sensitivity of Gd^{3+}-nitroxide and Gd^{3+}- Gd^{3+} DEER experiments. Abbreviations as for Table 2. Estimated number of paramagnetic centres per AuNP is 0.4 for nitroxide radicals and 3.2 for Gd^{3+} centres.

	Gd-NO @ Xband	Gd-NO @ Qband	Gd^{3+}-Gd^{3+} @ Qband
Modulation depth	0.15	0.16	0.037
srt [μs]	2040.00 us	897.60 us	897.60 us
point per trace	280	355	355
spp in single trace	30	200	100
length of pcp	16	16	16
scans	231	23	40
rmsd	4.4e-003	1.6e-003	2.6e-004
S/N	34.8	97.5	141.4
S/N per shot	3.1e-004	1.3e-003	2.2e-003

As explained in section 1, the average composition of functionalized AuNPs was determined to be $\mathbf{Au_{439}L_{80}NO_{0.2\text{-}0.4}}$. Thus 2% Gd^{3+} loading would correspond to approximately 1.6 Gd^{3+} centres per AuNP and 4% Gd^{3+} loading would correspond to an average of 3.2 Gd^{3+} centres per AuNP. The observed nitroxide-nitroxide DEER modulation depth for both 2% and 4% Gd^{3+}-loaded samples suggests a fraction of nitroxide-nitroxide pairs of about 40% of the total number of nitroxide labelled AuNPs. Assuming a uniform distribution of nitroxides over all AuNPs, this suggests an average of about 0.4 active nitroxides per AuNP. This estimate is also in line with the modulation depths observed in the Gd^{3+}-nitroxide DEER measured on these samples.

In Table 2, assuming a ratio of 1:4 for the numbers of nitroxides and Gd^{3+} ions per one AuNP, the sensitivity of Gd^{3+}-nitroxide DEER is slightly lower than for the nitroxide-nitroxide DEER, if computed per shot per unit spin concentration. Due to the faster longitudinal relaxation of Gd^{3+} ions, the sensitivities of the two types of DEER experiment are nearly the same if computed per unit time and per unit spin concentration.

To compare the sensitivities of Gd^{3+}-nitroxide and Gd^{3+}- Gd^{3+} DEER measurements (Table 3) it is necessary to take into account the reduced number of Gd^{3+}-nitroxide pairs, since there exist not more than 0.4 active nitroxides per AuNP. It has not been experimentally shown that the modulation depth in Gd^{3+}-nitroxide DEER can reach the same values as in nitroxide-nitroxide DEER (about 0.5 for 100% of spin pairs), but the available experimental data are in line with this assumption. If corrected for this potential increase, the sensitivity of Gd^{3+}-nitroxide DEER at Q-band could increase according to the increase of the DEER modulation depth, i.e. by a factor of 0.5/0.16≈3. This would lead to about twice better sensitivity for Gd^{3+}-nitroxide DEER as compared to the Gd^{3+}- Gd^{3+} DEER. One can expect that the relative sensitivities of the three types of distance measurements may change depending on the sample under study.

5. T_1 and T_2 times of Gd^{3+} ions and nitroxide radicals

The longitudinal relaxation times of Gd^{3+} species at 10 K and nitroxide radicals at 50 K were measured with the inversion recovery experiment. The corresponding 1/e decay times were about 270 μs for Gd^{3+} ions and 750 μs for nitroxide radicals. The corresponding transverse relaxation times for both species measured with variable interpulse delay Hahn echo pulse sequence are shown in Fig. S15.

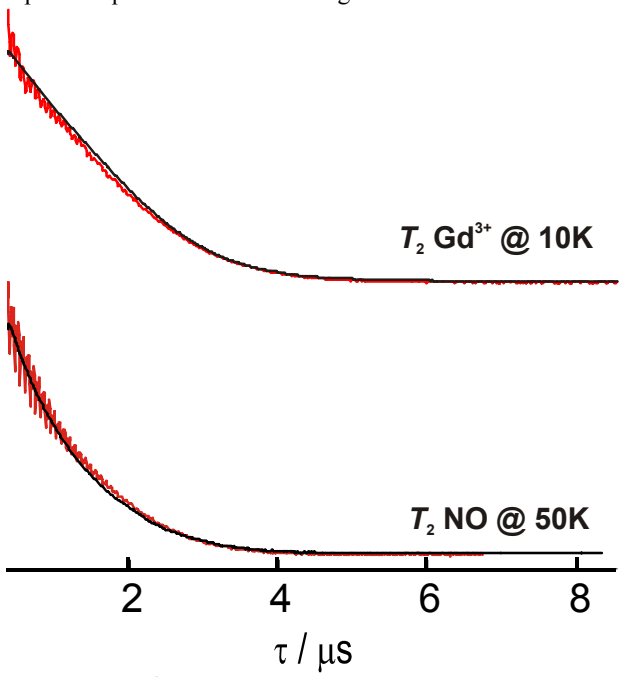

Figure S15. T_2 measurements for Gd^{3+} (above) and nitroxide radicals (below) performed at the temperatures of corresponding DEER experiments (10 K for Gd^{3+} ions, 50 K for nitroxide radicals): red: X-band measurements; black: Q-band measurements. Sample: 2% Gd^{3+} loaded. Pulse settings for nitroxide radicals: π/2=16 ns, π=32 ns; for Gd^{3+} ions: π/2=12 ns, π=24 ns.

6. Echo reduction effect and its tentative interpretation

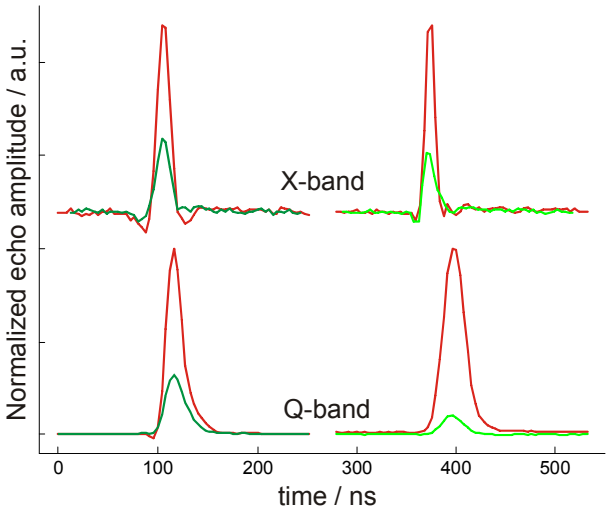

Figure S16. Comparison of the DEER echo reduction upon switching on the pump pulse.The left column shows results for the setup with the pump pulse at the maximum of the nitroxide spectrum (+80 MHz at X band, +300 MHz at Q band). In this case the position of the pump pulse corresponded to the magnetic field to the left of the detection field. In the right column the echo reduction for the mirrored setup is shown. In this case the pump pulse position was to the right from the detection field. At that position no nitroxide species could be excited. Standing DEER sequence: $\tau_1 = 400$ ns, $\tau_2 = 1200$ ns; the pump pulse was set to come on top of the primary echo. Measurements with $\tau_2 = 3000$ ns resulted in approximately the same magnitudes of echo reduction. The difference in echo reduction between the cases $\tau_2 = 1200$ ns and $\tau_2 = 3000$ ns was within the estimated experimental error.

The qualitative mechanism of the DEER echo reduction can be proposed as follows. If the pump pulse hits a transition that has a level in common with the transition on which the detection takes place, part of the coherence is transferred to other elements of the density matrix and is not detected later in the experiment. The illustrations are given for the case, when detection frequency is in resonance with the $|-1/2\rangle \leftrightarrow |+1/2\rangle$ transition.

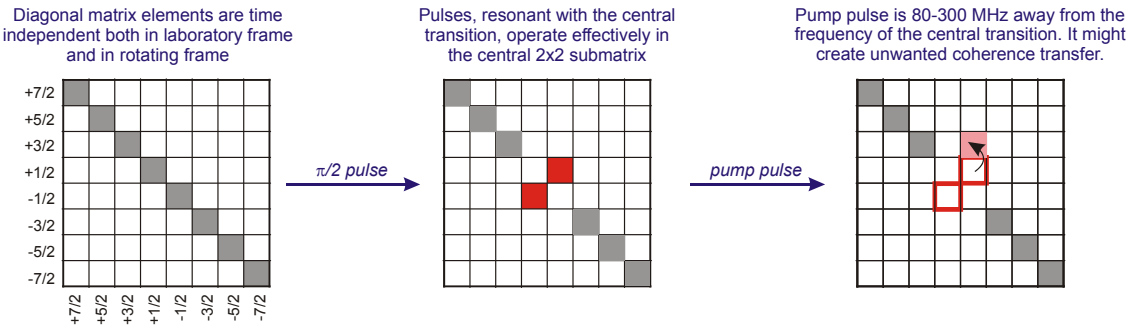

Figure S17. Tentative mechanism of the echo reduction in Gd^{3+}-nitroxide DEER experiment.

The reduction of the coherence on the central transition upon applying the pump pulse 300 MHz apart from the frequency of detection pulses has been analysed in a model calculation. The frequency offset used in this calculation corresponds to the experimental conditions at Q-band. A coherence on the central transition of the Gd^{3+} center was created by applying a resonant $\pi/2$ pulse. After that an effect of the pump pulse on this coherence was tested. No evolution period between $\pi/2$ and pump pulses has been computed for Fig. S18. A

single orientation of the ZFS-tensor with its Z-axis along the direction of B-field has been considered. The strongest echo reduction is observed when the pump pulse "hits" both |1/2> ↔ |3/2> and |3/2> ↔ |5/2> transitions of the Gd^{3+} center.

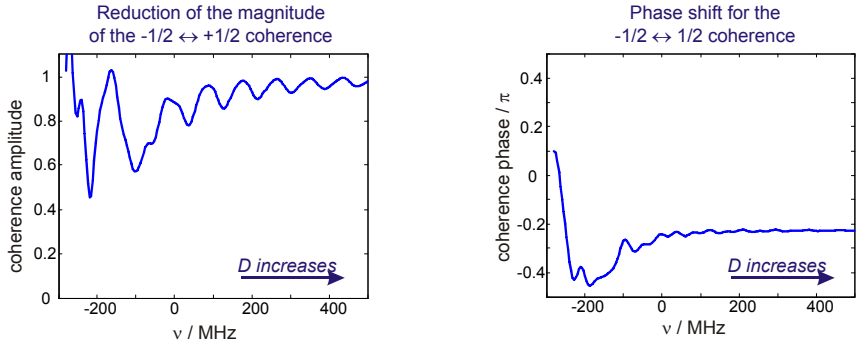

Figure S18. Reduction of the magnitude and change of the phase for the coherence on the central transition of Gd^{3+} for the collinear and axially symmetric ZFS and EZ interactions upon the application of a pump pulse. Frequency ν (x-coordinate in both figures) is the offset between the |+1/2> ↔ |+3/2> transition frequency and the pump frequency. Negative values mean that the pump frequency is higher than the frequency of the |+1/2> ↔ |+3/2> transition.

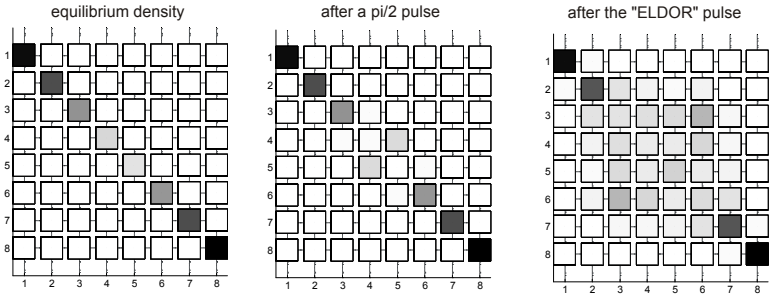

Figure S19. Numerically calculated density matrix evolution in the standing DEER pulse-sequence for the case ν = -200 MHz. ZFS and EZ terms were oriented as for Fig. S18. The standing DEER pulse sequence including all time evolution periods was computed up to the time point just after the pump pulse. Lengths of all pulses were set to 12 ns, the first interpulse delay τ_1 in the pulse sequence was set to 400 ns.

The presented calculations only confirm the possibility of the echo reduction with the proposed mechanism. Systematic work on analysing the dependence of this effect on the orientation of the ZFS tensor with respect to the external magnetic field and on the strength and distribution of ZFS parameters is currently in progress and will be reported in a separate publication.

As an example we estimated the echo reduction for the model distribution of D and E parameters of the ZFS tensor that we used for the ED EPR spectra simulations and for the calculations of excited dipolar frequencies. For that we performed a full DEER sequence calculation for an ensemble of randomly oriented Gd^{3+} centers with Gaussian distribution of D-values (<D>=1500 MHz, σ(D)=D/10) and with the polynomial distribution of E/D-values as described in the main article. The calculations were performed in the laboratory frame. This approach is too demanding for Q-band, because of very high transition frequencies. The direct calculations were done for X-band settings: B = 3400 G, detection frequency – 9.474 GHz, pump frequency – 9.389 GHz, all pulses rectangular with the 12 ns duration, first interpulse delay – 400 ns, second interpulse delay (between the primary echo and the refocusing pulse) – 1200 ns. The time position of the pump pulse was selected to coincide with the position of the primary echo. With these settings we performed a 72000-steps Monte-Carlo calculation

of the DEER echo in presence and in absence of the pump pulse. The results of this calculation are shown in Fig. S20. The obtained reduction of the DEER echo is about 50%, which slightly underestimates the degree of the echo reduction observed in experiment for given conditions. The computed reduction of the DEER echo amplitude accounts for both Bloch-Siegert shift[S1,S2] and for the effect due to the high spin features of Gd^{3+} centers mentioned above. In contrast to the short communication that appeared during the revision of this manuscript,[S3] where only the Bloch-Siegert shift was analysed and a rough approximation for the differences in transition moments for different transitions of Gd^{3+} centers was made, our calculation is exact for given parameters of the spin Hamiltonian. Therefore the remaining difference between the calculated and the experimental degree of DEER echo reduction is attributed to the approximations done for the spin Hamiltonian parameters of Gd^{3+} centers.

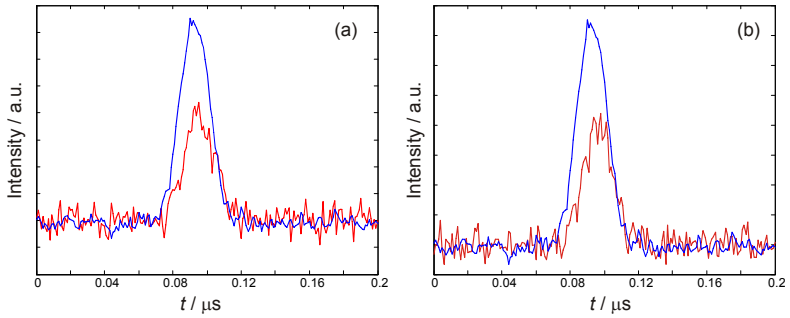

Figure S20. Calculation of the Gd^{3+} DEER echo with (red) and without (blue) pump pulse. D = 1500 MHz (σ=D/10); Magnetic field B_0=3400 G, ν_{det}=9.474 GHz, ν_{pump}= ν_{det} - 85 MHz (a) ν_{pump}= ν_{det} + 85 MHz (b). 72000 shots (~15.2 hours computation time for each calculation); All pulses 12 ns, detection pulses tuned for Gd^{3+}, pump pulse tuned for nitroxide radicals (4π flip angle for Gd^{3+} centers); first delay time τ_1=400ns; second delay time τ_2=1200ns; 5000 steps propagation for each pulse.

7. DEER measurements at X and Q band

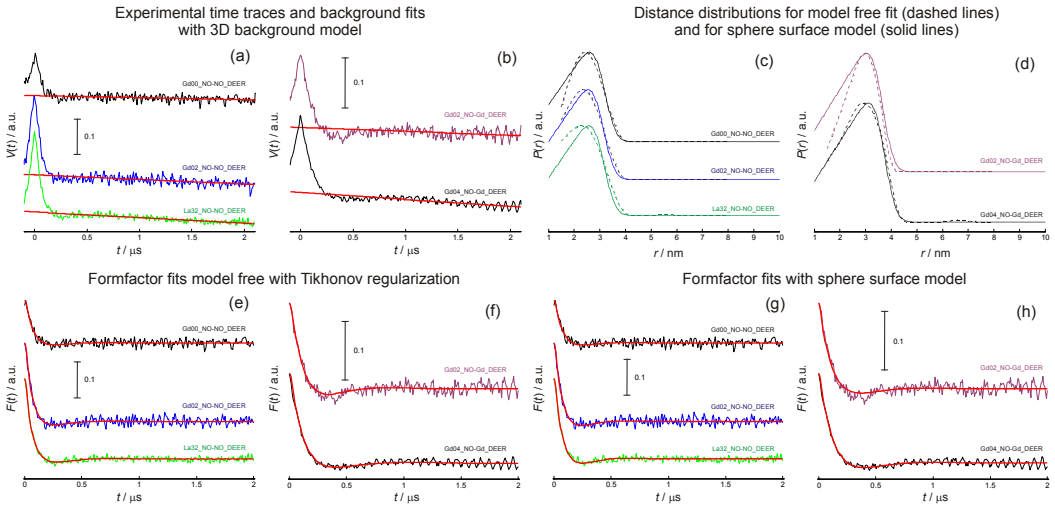

Figure S21. X-band DEER measurements and their analysis: (a) – primary experimental nitroxide-nitroxide DEER traces for the AuNPs with 0% (black) and 2% (blue) Gd^{3+} load and with 32% load of La^{3+} (green), the background fits are shown in red; (b) – primary experimental Gd^{3+}-nitroxide DEER traces for the AuNPs with 2% (purple) and 4% (black) Gd^{3+} load, the background fits are shown in red; (c) – distance distributions obtained from the nitroxide-nitroxide DEER traces after fitting them with DeerAnalysis, using the single sphere model (solid lines) and model free fit with Tikhonov regularization (dashed lines), color code as for experimental traces in (a); (d) – distance distributions obtained from the Gd^{3+}-nitroxide DEER traces after fitting them with DeerAnalysis, using the single sphere model and model free fit with Tikhonov regularization, color code as in (b); (e) – background corrected form factor signals for the nitroxide-nitroxide DEER and their model free fits (red) with Tikhonov regularization, color code for experimental traces as in (a); (f) – background corrected form factor signals for the Gd^{3+}-nitroxide DEER and their model free fits (red) with Tikhonov regularization, color code for experimental traces as in (b); (g) – background corrected form factor signals for the nitroxide-nitroxide DEER and their sphere surface model fits (red), color code for experimental traces as in (a); (h) – background corrected form factor signals for the Gd^{3+}-nitroxide DEER and their sphere surface model fits (red), color code for experimental traces as in (b);

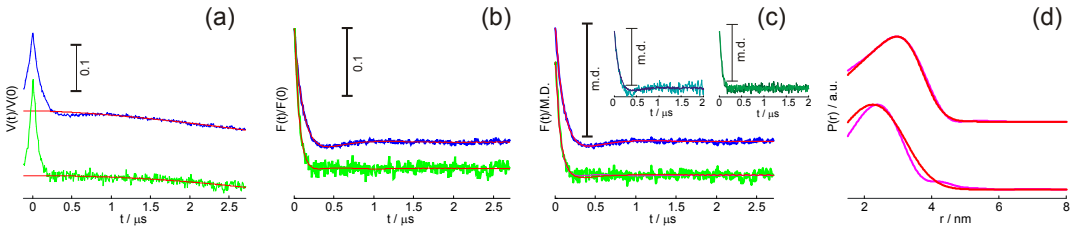

Figure S22. Q-band DEER measurements on 2% Gd^{3+}-loaded AuNPs and their analysis: (a) – primary experimental Gd^{3+}-nitroxide (blue) and nitroxide-nitroxide (green) DEER traces, the background fits are shown in red; (b) model free DEER form factor fits with Tikhonov regularization (red), the color code for experimental traces as in (a); (c) – sphere surface model DEER form factor fits (red), the color code for experimental traces as in (a); left inset – comparison of the X- band (cyan) and Q-band (black) nitroxide-nitroxide DEER traces for this sample; right inset – comparison of the X- band (dark green) and Q-band (black) Gd^{3+}-nitroxide DEER traces for this sample; (d) – distance distributions obtained from sphere surface model fit (red) and from the model free fit with Tikhonov regularization (pink), the upper two distributions were calculated for the Gd^{3+}-nitroxide DEER trace, the lower two distributions were calculated for the nitroxide-nitroxide DEER trace.

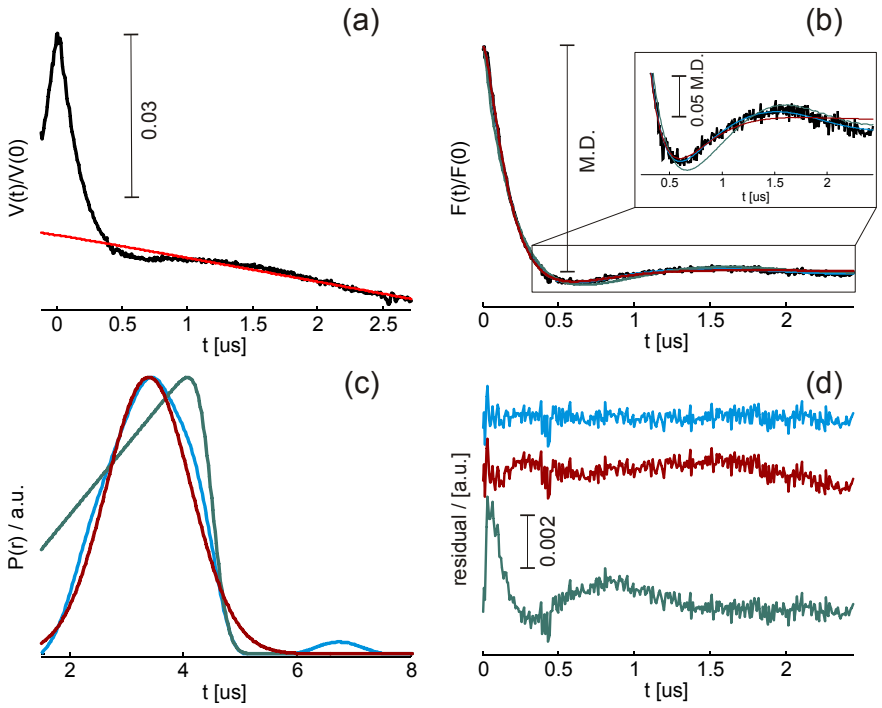

Figure S23. Distance analysis of the Gd^{3+}-Gd^{3+} DEER measurement (4% Gd^{3+} loaded sample). (a) experimental DEER time trace (black) and background fit (red); (b) the background corrected form factor signal (black) and its fit with model free Tikhonov regularization procedure (blue), with a Gaussian distribution (dark red) and with the sphere surface model (dark green); (c) obtained distance distributions for the model free fit (blue), Gaussian fit (dark red) and the sphere surface model fit (dark green); (d) residuals after subtraction of the form factor signal from the fit results, color code as in (b) and (c).

References:

(S1) F. Bloch, A. Siegert, *Phys. Rev.* 1940, **57**, 522–527.
(S2) M.K. Bowman and A.G. Maryasov, *J. Magn. Reson.*, 2007, **185**, 270–282.
(S3) I. Kaminker, H. Yagi, T. Huber, A. Feintuch, G. Otting and D. Goldfarb, *Phys. Chem. Chem. Phys.*, 2012, **14**, 4355–4358.